Journal of Solid State Chemistry 188 (2012) 84–91

Contents lists available at SciVerse ScienceDirect

Journal of Solid State Chemistry

journal homepage: www.elsevier.com/locate/jssc

Thermal expansion of $Ba_2ZnSi_2O_7$, $BaZnSiO_4$ and the solid solution series $BaZn_{2-x}Mg_xSi_2O_7$ ($0 \le x \le 2$) studied by high-temperature X-ray diffraction and dilatometry

Marita Kerstan, Matthias Müller, Christian Rüssel *

Otto-Schott-Institut, Jena University, Fraunhoferstr. 6, 07743 Jena, Germany

ARTICLE INFO

Article history:
Received 3 November 2011
Received in revised form
24 January 2012
Accepted 26 January 2012
Available online 4 February 2012

Keywords:
Barium zinc silicates
Barium magnesium zinc silicates
Thermal expansion
High-temperature X-ray diffraction
dilatometry

ABSTRACT

The thermal expansion behavior of $Ba_2ZnSi_2O_7$, $BaZnSiO_4$ and $BaZn_2Si_2O_7$ is characterized by both high-temperature X-ray diffraction (HT-XRD) and dilatometry. $Ba_2ZnSi_2O_7$ and $BaZnSiO_4$ show a thermal expansion (100–800 °C) in the range from 8.9 to 10.4 $\times$ 10^{-6} K^{-1}. By contrast, $BaZn_2Si_2O_7$ has a much higher thermal expansion in the low-temperature modification and shows a phase transition at 280 °C which runs parallel with a steep increase in cell volume. This phase transition is also observed in the solid solution series $BaZn_{2-x}Mg_xSi_2O_7$, but it is shifted to higher temperatures and to a smaller volume change with increasing Mg^{2+} concentration. This solid solution series is characterized by dilatometry, X-ray diffraction and differential scanning calorimetry. An adjustment of the MgO/ZnO-ratio enables the preparation of materials with a large variety of thermal expansions.

© 2012 Elsevier Inc. All rights reserved.

1. Introduction

For the preparation of gas-tight and electrically insulating seals glass or materials derived hereof are often used [1]. For this purpose, the first step of the preparation procedure is the melting of a glass. Then the glass is crushed and powdered and brought in between the two components which should be joined. Heating to elevated temperatures leads to a sintering process.

If the sealing materials should have high thermal expansion coefficients ($\ge 10 \times 10^{-6}$ K^{-1}) and be applied at high temperatures, glasses are hardly suitable as sealing materials, because glasses with high softening temperatures usually possess a low thermal expansion coefficient. The problem of temperature stability vs. high thermal expansion might be overcome by a subsequent annealing step during which crystalline phases with high thermal expansion coefficients are precipitated. This procedure is e.g., required if the glass should be used for solid-oxide fuel cells (SOFCs) or high temperature reactors. Here, the glass has to withstand high temperatures as well as thermal cycling and has to be stable over a long period of time (many years) at high temperatures. For this purpose, the softening temperature should be higher than the operating temperature and the thermal expansion coefficients (CTEs) of the seal glass (after crystallization) and of the different components of the cell should match within $\pm 1 \times 10^{-6}$ K^{-1}.

One important issue of crystallizing glass seals is the adjustment of the flow behavior which is quite essential for the sintering and the crystallization process. It is controlled by the chemical composition, including the addition of nucleating agents or nucleation inhibitors. The sintering process as well as the crystallization process is furthermore affected by the temperature time schedule.

Another possibility for SOFCs is to attach a compressive load to the components [2]. In between these components, crystalline powders, e.g., based on mica are given in Refs. [3–5].Sang et. al. reported the leak rate of such systems, which might be low enough to be suitable in application in a SOFC. Although compressive seals might show a good performance, the technical afford especially to apply an external load is fairly high [1].

For components of a solid oxide fuel cell (SOFCs), various materials have been proposed. As solid electrolyte, stabilized zirconia (in tetragonal or cubic modification) is widely used; the linear thermal expansion coefficients (30–800 °C) are in the range from 10.3 to 10.6 $\times$ 10^{-6} K^{-1} [6], depending on the dopants (e.g., magnesia, ceria or yttria). As cathode material various perovskites with mixed anionic (O^{2-}) and electronic conductivity might be used, One example are $La_{1-x}Sr_xCoO_{3\pm\delta}$ ceramics which have a CTE (30–700 °C) in the range from 11 to 14 $\times$ 10^{-6} K^{-1} for x=0.15–0.5 [7]. The common anode material is a cermet of nickel and yttrium-stabilized zirconia with a CTE (30–1000 °C) of

* Corresponding author.
E-mail address: ccr@rz.uni-jena.de (C. Rüssel).

0022-4596/$ - see front matter © 2012 Elsevier Inc. All rights reserved.
doi:10.1016/j.jssc.2012.01.055

12.6 × 10^{-6} K^{-1} [8]. As interconnect, most frequently ferritic steels with CTE of typically 12.3 × 10^{-6} K^{-1} (20–25% chromium) [9] are used.

The most interesting temperature-stable phases which exhibit high CTEs are based on alkaline earth silicates. These crystalline phases can either be used as fillers or, however, they can directly be crystallized from suitable glass compositions. A crystal phase with a high CTE as a component of a sealing material increases the CTE of the seal (which should lie in between the CTEs of its constituents, i.e., all crystalline phases and possibly a residual glassy phase). In the literature, some studies on CTE of alkaline earth silicates as well as of zinc silicates have already been reported. Up to now, mostly binary crystalline phases in the systems BaO–SiO_2 [10], CaO–SiO_2 [11,12] and ZnO–SiO_2 [11] have been considered. Besides, the CTE of some ternary crystalline phases in the systems BaO–CaO–SiO_2 and CaO–ZnO–SiO_2 and one quarternary barium calcium zinc silicate [11] have been reported.

In the system BaO–ZnO–SiO_2 a ternary phase diagram with five ternary phases was described by Segnit and Holland [13] (see Fig. 1). The phase formation in the binary system BaO–SiO_2 was already revised by other authors (e.g., [14]). The ternary system

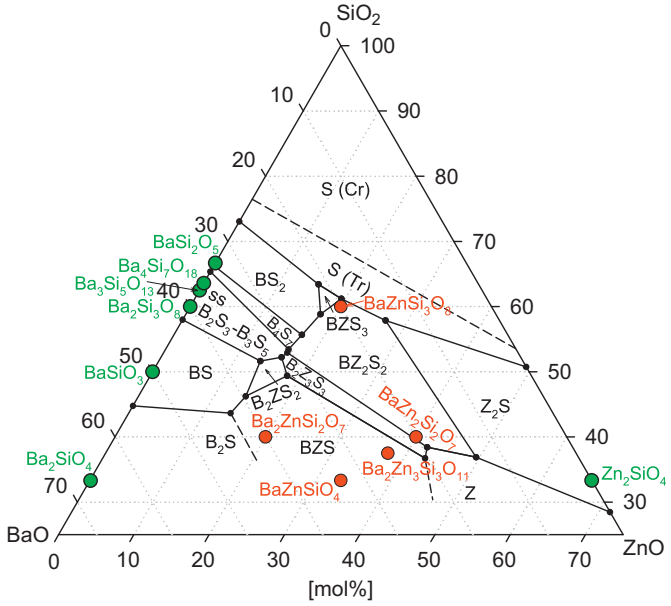

Fig. 1. Ternary phase diagram of the system BaO–ZnO–SiO_2 as determined by Segnit [13]. Binary phases – green; ternary phases – red; phase stability fields – black (B: BaO; Z: ZnO; S: SiO_2; Cr: Cristobalit; Tr: Tridymit).

needs further revision, because the existence of only three ternary phases could be proved and a crystal structure was described later: $Ba_2ZnSi_2O_7$ [15], $BaZnSiO_4$ [16] and $BaZn_2Si_2O_7$ [17]. Up to now only for the latter phase, cell parameters at various temperatures from 25 to 900 °C have been reported (see Lin et al. [17]). This phase shows a phase transition at about 280 °C which runs parallel to a large volume expansion. This phase shows the same crystal structure as $BaMg_2Si_2O_7$ [18] and solid solutions of those two phases should be possible. The phase transition should also be affected by the formation of the solid solution with respect to both, the attributed temperature and the volume effect.

This paper reports on the thermal expansion behavior of barium zinc silicates studied by both high temperature X-ray diffraction and dilatometry and solid solutions of $BaZn_2Si_2O_7$ and $BaMg_2Si_2O_7$ studied by dilatometry.

2. Materials and methods

The silicates were prepared from reagent grade raw materials. Mixtures of SiO_2 (quartz powder C, SCHOTT), $BaCO_3$ (chemical pure, REACHIM), ZnO (for analysis, FERAK) and 4 $MgCO_3 \cdot Mg(OH)_2 \cdot 2\ H_2O$ (extra pure, MERCK) were ball milled and thermally annealed at 1250–1475 °C for 2 to 8 h (barium zinc silicates) or at 1200–1360 °C for 5 to 8 h (solid solution series $Ba_{2-x}Mg_xSi_2O_7$ with $x=0.1$; 0.2; 0.5; 1.0; 1.5 and 2.0). After cooling, the samples were ball milled again. This procedure was repeated at least twice. The phase compositions were controlled by X-ray powder diffraction (XRD), using a SIEMENS D5000 diffractometer with Cu K_α radiation. Each sample was measured at $10 \le 2\theta \le 60°$ with a step width of 0.02°. The XRD-patterns were analyzed using the software *DIFFRAC.EVA* from BRUKER.

High-temperature X-ray diffraction (HT-XRD) was performed using a SIEMENS D5000 diffractometer with an ANTON PAAR *HTK 10* heating stage, suitable for temperatures up to 1000 °C. All XRD samples were previously ball milled in order to obtain a grain size < 63 µm. The samples were heated using a rate of 10 K/s and kept at various temperatures for several minutes until temperature equilibrium was established. Then the XRD-patterns were recorded within 30 min (counting time: 1 s, step size: 0.02°). Subsequently, the sample was heated (or cooled) to a new temperature and the next measurement was started. From the XRD-patterns, cell parameters for each temperature were determined by Rietveld method (but without refinement of the atom coordinates) using software *TOPAS* from BRUKER. The starting values for the crystal structure data were taken from the Inorganic Crystal Structure Database (ICSD) [16–17] (see also Table 1).

Table 1
Cell parameters for the barium zinc silicates and $BaMg_2Si_2O_7$ at room temperature in comparison to literature values (N–standard sample holder, HS–heating stage).

Phase	*a* (Å)	*b* (Å)	*c* (Å)	*β* (°)	*V* (Å³)	Source
$Ba_2ZnSi_2O_7$	8.43311(92)	10.72788(91)	8.44694(90)	110.9912(49)	713.47(13)	Standard
C 2/c (15)	8.4235(18)	10.7152(15)	8.4390(16)	110.9985(98)	711.11(23)	Heating stage
Monoclinic	8.434(2)	10.722(2)	8.436(2)	111.30(3)	710.75	ICSD 409588 [15]
$BaZnSiO_4$	9.09462(3)	*9.09462(3)*	8.7265(32)	*90*	625.086(48)	Standard
P 6_3 (1 7 3)	9.0972(24)	*9.0972(24)*	8.7261(24)	*90*	625.420(37)	Heating stage
Hexagonal	9.0850(9)	9.0850(9)	8.7147(11)	*90*	622.92	ICSD 73777 [16]
$BaZn_2Si_2O_7$ LT	7.27796(55)	12.79949(94)	13.68681(90)	90.1077(66)	1274.98(16)	Standard
C 2/c (15)	7.2605(18)	12.7796(33)	13.6574(31)	90.064(24)	1267.22(53)	Heating stage
Monoclinic	7.2782(4)	12.8009(7)	13.6869(7)	90.093(6)	–	[17]
$BaZn_2Si_2O_7$ HT	–	–	–	–	–	Standard
C c m 2_1 (36)	7.6049(20)	12.9940(34)	6.7217(26)	*90*	664.23(36)	Heating stage (300 °C)
Orthorhombic	7.6199(4)	13.0265(6)	6.7374(2)	*90*	–	ICSD 88589 [17] (280 °C)
$BaMg_2Si_2O_7$	7.24256(43)	12.71085(81)	13.75066(81)	90.1900(53)	1265.87(13)	Standard
C 2/c (15)	–	–	–	–	–	Heating stage
Monoclinic	7.24553(8)	12.71376(14)	13.74813(15)	90.2107(8)1	1266.44(2)	[18]

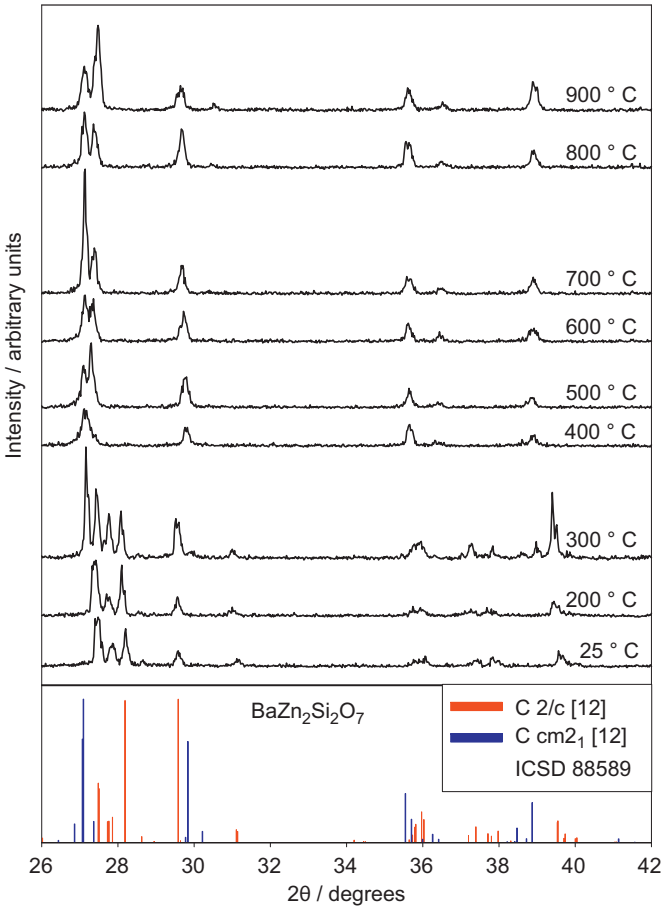

Fig. 2. XRD-patterns of $BaZn_2Si_2O_7$ measured at different temperatures. The lower part of the graph shows the literature values of both the monoclinic low-temperature and the orthorhombic high-temperature modification of $BaZn_2Si_2O_7$ [17].

For the preparation of samples for dilatometric measurements, the respective silicate powders (grain size < 63 μm) were cold isostatically pressed (200–250 bar, 20–30 s) to cylindrical shape (diameter: 6–8 mm, length: 6–20 mm). In order to sinter these materials, the samples were re-heated for 5 to 12 h to 1000–1200 °C. In the case of $BaZn_2Si_2O_7$, thermal annealing was not carried out, because a phase transformation occurred at about 280 °C. The dilatometric measurements (heating rate 5 K/min) were done using a dilatometer NETZSCH *Dil 402 PC*.

The differential scanning calometry (DSC) was carried out at a METTLER TOLEDO *DSC 822e* with a heating rate of 10 K/min.

3. Results

Fig. 2 shows the XRD-patterns of $BaZn_2Si_2O_7$. The patterns recorded at room temperature show distinct lines all attributable to the monoclinic low-temperature phase $BaZn_2Si_2O_7$ [17]. At 200 °C, the pattern is fairly similar and a slight shift of the lines is observed, e.g., the three strongest reflections are shifted from 27.48 to 27.42°, 28.20 to 28.10° and from 27.86 to 27.78°. At 300 °C additional lines occur, which represent the orthorhombic high-temperature phase (ICSD 88589 [17]). At temperatures in the range from 400 to 900 °C, all observed lines are attributable to this high-temperature phase. The changes in Bragg angles are quite different for the three strongest reflections. The strongest line is slightly shifted from 27.16 to 27.10° during heating from 300 to 500 °C. After further heating, the Bragg angle remains nearly constant (27.14 at 800 °C, 27.12 at 900 °C). The other XRD lines show more notable changes: one is shifted to smaller Bragg angles (from 29.82° at 400 °C to 29.64° at 900 °C); another is shifted to larger Bragg angles (27.3° at 500 °C to 27.48° at 900 °C).

Another behavior is observed in the cases of $BaZnSiO_4$ and $Ba_2ZnSi_2O_7$. All recorded X-ray diffraction patterns at each temperature show only reflections attributable to crystalline $Ba_2ZnSi_2O_7$ [15] and $BaZnSiO_4$ [16]. All reflections of those patterns are shifted to smaller Bragg angles with increasing temperature.

Table 1 summarizes the cell parameters of all studied samples at room temperature (determined by Rietveld algorithm), both measured on the heating stage and on the standard sample holder. The deviations of the cell parameters measured at room temperature (see Table 1) were in the range from −0.05 to 0.61%.

The cell parameters determined by Rietveld calculations were plotted against the temperature (see Fig. 3 for the examples of $BaZnSiO_4$) and fitted to a polynomial function of the form $y = y_0 + n \cdot T + m \cdot T^2$ or $y = y_0 + n \cdot T$ (which is common in literature, see for example [19]) using a least square fit approximation. The temperature is in °C and hence, the fit parameter y_0 represents the respective cell parameter at 0 °C, the fit parameters n and m represent the effect of temperature. The parameters determined using the Rietveld algorithm are shown as circles while the polynomial fits are shown as dashed lines. In Table 2 the fitted cell parameters of the barium zinc silicates and their temperature dependencies are summarized.

In Fig. 4, the relative changes in cell parameters of the barium zinc silicates are shown as a function of temperature, calculated as $\Delta y/y_{25} = (y_T - y_{T=25°C})/y_{T=25°C}$, where y is the respective cell parameter either directly received from Rietveld refinement (see the symbols) or calculated from the polynomial fit (see the lines). The attributed CTEs (calculated as $\alpha_y = 1/y_{T1} \cdot (y_{T2} - y_{T1})/(T_2 - T_1)$, where y is the cell parameter calculated from the polynomial fit, T_1 is 100 °C, T_2 is 800 °C) are shown in Table 3. With the exception

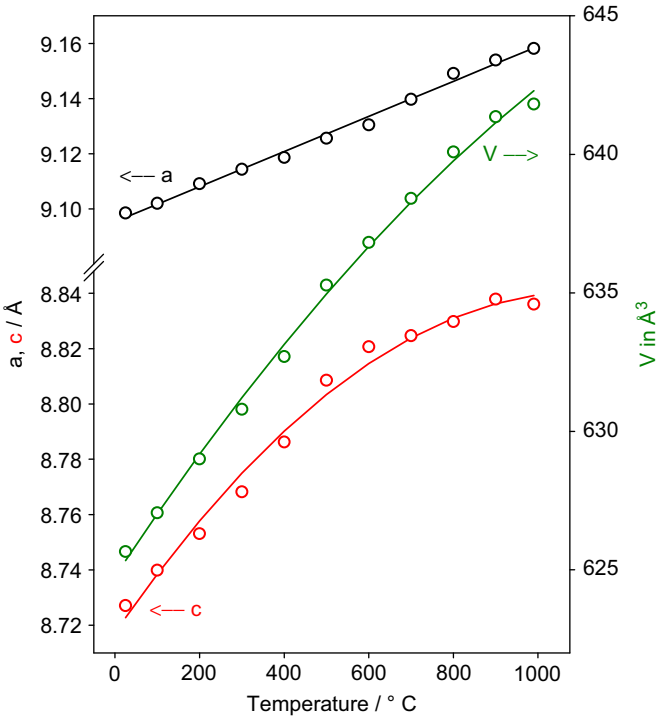

Fig. 3. Cell parameters determined by Rietveld method (circles) of $BaZnSiO_4$ as a function of temperature and polynomial fit (solid line). For regression coefficients see Table 2.

Table 2
Cell parameters of the barium zinc silicates and their temperature dependencies.

Cell parameter			Sample											
			$Ba_2ZnSi_2O_7$		$BaZnSiO_4$		$BaZn_2Si_2O_7 < 300$ °C		$BaZn_2Si_2O_7 < 300$ °C [17]		$BaZn_2Si_2O_7 > 300$ °C		$BaZn_2Si_2O_7 > 280$ °C [17]	
	Regression parameter		Value	Std. err.	Value	Std. err.	Value	Std. err.	Value	Std. err.	Value	Std. err.	Value	Std. err.
a	y_0	(Å)	8.4245	0.0021	9.0953	0.0010	7.2538	0.0075	7.2750	0.0023	7.7218	0.0242	7.7508	0.0157
	n	(10^5 Å/K)	3.74	1.23	6.37	0.18	18.60	3.58	19.58	0.97	−48.21	8.66	−55.18	6.06
	m	(10^9 Å/K^2)	3.32	1.45	–	–	–	–	–	–	29.12	7.14	31.96	5.23
b	y_0	(Å)	10.7132	0.0008	–	–	12.7730	0.0001	12.7938	0.0019	12.9853	0.0094	13.0018	0.0031
	n	(10^5 Å/K)	9.71	0.18	–	–	26.52	0.04	33.48	0.81	6.83	1.68	9.96	0.59
	m	(10^9 Å/K^2)	–	–	–	–	–	–	–	–	–	–	–	–
c	y_0	(Å)	8.4350	0.0019	8.7172	0.0038	13.6506	0.0168	13.6881	0.0037	13.3546	0.0062	13.3860	0.0092
	n	(10^5 Å/K)	5.51	0.41	20.00	1.80	8.77	8.06	5.86	1.60	30.00	1.11	34.44	1.73
	m	(10^9 Å/K^2)	–	–	−10.04	1.73	–	–	–	–	–	–	–	–
B	y_0	(°)	110.992	0.008	–	–	90.074	0.046	n. d.	–	–	–	–	–
	n	(10^4 °/K)	−4.87	0.17	–	–	1.08	2.00	–	–	–	–	–	–
	m	(10^8 °/K^2)	–	–	–	–	–	–	–	–	–	–	–	–
V	*y0*	(Å^3)	710.46	0.20	624.76	0.29	1264.74	2.90	1273.15	0.52	1323.02	0.88	1334.83	1.17
	n	(10^2 Å^3/K)	1.90	0.04	2.32	0.13	6.72	1.39	7.90	0.22	1.39	0.16	1.05	0.23
	m	(10^6 Å^3/K^2)	–	–	−0.55	0.13	–	–	–	–	–	–	–	–

of $BaZn_2Si_2O_7$, where the already mentioned phase transition occurs, the cell parameters increase steadily with the temperature. In the case of $BaZnSiO_4$, the CTE with respect to the crystallographic *a*- and *c*-axes are 7.0 and 15.1 · 10^{-6}/K, respectively. The mean thermal expansion coefficient α_m is calculated as the mean of the expansions in the three orthogonal directions of the unit cell (in orthorhombic systems *a*, *b* and *c*, in hexagonal systems twice *a* and *c* and in monoclinic systems *a*, *b*, $h=c \cdot \sin\beta$. For $BaZnSiO_4$ the mean CTE is 9.7 · 10^{-6}/K. Here, the thermal expansion is strongly anisotropic and in the direction of the crystallographic *c*-axis more than twice as large as in the other crystallographic direction.

By contrast, concerning $Ba_2ZnSi_2O_7$, the CTEs are 8.0, 9.1 and 6.5×10^{-6}/K with respect to the crystallographic *a*−, *b*−, and *c*-axes, respectively, and hence the dependency on the crystallographic direction is much smaller. The smallest CTE along the *c*-axis has 72% of the highest CTE (*b*-axis). The mean thermal expansion α_m is $8.9 \cdot 10^{-6}$/K (it is not equal to the mean of α_a, α_b and α_c because of the changes in the cell angle β, for calculation of α_m please see above).

$BaZn_2Si_2O_7$ shows the highest thermal expansion and the highest anisotropy, not only because of the phase transition at about 280 °C. Also in the temperature range up to 300 °C, the mean thermal expansion α_m is about 1.5 and 2 times higher than those of $Ba_2ZnSi_2O_7$ and $BaZnSiO_4$, respectively, the expansion of the cell parameters *a* and *b* is even about four times higher than those of the respective axes of $Ba_2ZnSi_2O_7$ and $BaZnSiO_4$. Taking into account the phase transition, the mean thermal expansion α_m of $BaZn_2Si_2O_7$ is 2.5 times as large as α_m of the other two barium zinc silicates, although the expansion of the *c*-axis of $BaZn_2Si_2O_7$ is even negative. Calculating the thermal expansion only at the phase transition (300 °C), it is 4.0% for the *a*-axis, 1.2% for the *b*-axis, -1.7% for the *c*-axis, which results in 3.5% for the volume. The CTE of the high-temperature modification is largest for the *c*-axis. In the direction of the *b*-axis, the CTE is only one fourth of that of the *c*-axis, while for the *a*-axis it is negative; the absolute value is approximately the same as for the *c*-axis.

Fig. 5 illustrates results from dilatometry of barium zinc silicates (lines) as well as the relative changes in the cell volume obtained from Rietveld calculations. For the compounds $Ba_2ZnSi_2O_7$ and $BaZnSiO_4$, dilatometric and Rietveld results are in good agreement as well as for $BaZn_2Si_2O_7$ up to a temperature of 320 °C. The volume effect which runs parallel to the transition of the low-temperature to the high-temperature modification is very similar for the Rietveld calculation and dilatometry. Strong deviations, however, are observed at temperatures the high temperature modification is stable. The CTEs determined by dilatometry (for calculation see above, here the measured sample length is taken as *y*) are also summarized in Table 3.

In Fig. 6, XRD-patterns (intensity normalized to the maximum intensity) of the solid solution series $BaZn_{2-x}Mg_xSi_2O_7$ recorded at room temperature are shown. In all these compounds, approximately the same XRD peaks are observed. However, they are shifted depending on the chemical composition and changed in their intensity. Up to $x=0.5$ (i.e., 25% of Zn^{2+} were replaced by Mg^{2+}) the powder patterns are similar to those of $BaZn_2Si_2O_7$, and the peaks are shifted to larger Bragg angles with increasing Mg^{2+} concentration, e.g., from 28.22 to 28.36° and from 27.54 to 27.68° for the two strongest reflections. The powder patterns of the samples with $x=1.0$ and $x=2.0$ (50 and 75% Zn^{2+} were replaced by Mg^{2+}) are similar to the powder pattern of $BaMg_2Si_2O_7$, and the peaks are shifted to smaller Bragg angles with increasing Mg^{2+} concentration, for $BaMg_2Si_2O_7$, however, the shift is again smaller. The two strongest XRD lines are shifted from 28.38 to 28.24° ($x=1.5$) and 28.30° ($x=2.0$) and from 27.62 to 27.48° ($x=1.5$) and 27.56° ($x=2.0$).

The lattice parameters calculated by Rietveld refinement are shown in Fig. 7. For the end members $BaZn_2Si_2O_7$ and $BaMg_2Si_2O_7$, the crystallographic data from literature [17,18] were used as starting values for the Rietveld calculations, in which the cell parameters, the scale factor and the zero error were refined. The atom coordinates were kept constant. For the samples containing both Zn^{2+} and Mg^{2+}, a new crystallographic data set was created, containing the mean of each cell parameter and each M^{2+} position (despite of the Ba^{2+} position) randomly occupied by 50% Zn^{2+} and 50% Mg^{2+} and used as the starting value for refining the parameters, the scale factor and the zero error. The cell parameter *c* increases with increasing Mg^{2+} concentration, within the samples with up to $x=1$ (50% Zn^{2+} replaced by Mg^{2+}) with a larger slope than within the samples with $x>1$. Cell parameter *a* remains almost constant up to $x=0.2$. From $x=0.2$ to 0.5, the observed decrease is larger than in the range from $x=0.5$ to 2.0. The cell parameter b increases up to $x=0.2$, but decreases for further increasing Mg^{2+}-concentrations. This decrease is stronger in the range from $x=1.0$ to 2.0.

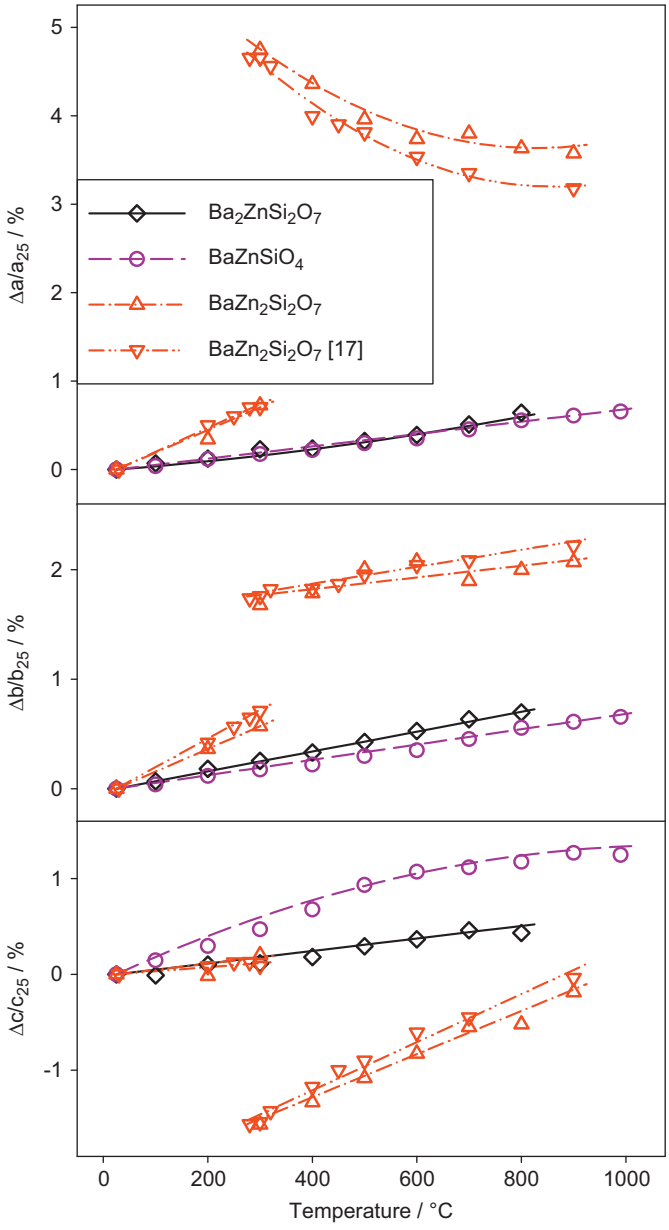

Fig. 4. Relative changes in cell parameters as a function of temperature as calculated from the polynomial fit of the cell parameters of the barium zinc silicates (please note: $BaZnSiO_4$ has a hexagonal unit cell and hence $a=b$.

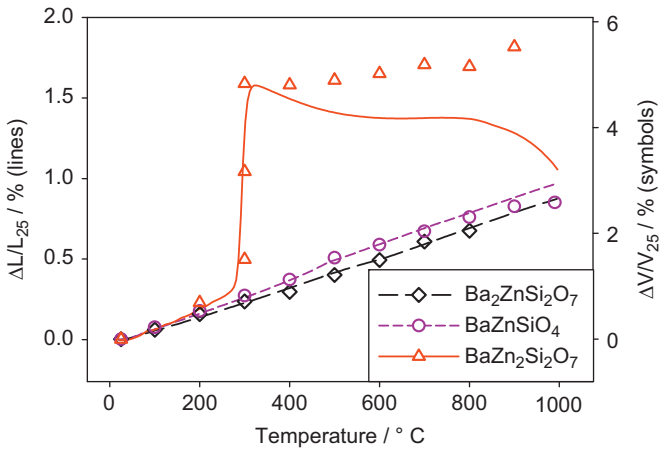

Fig. 5. Dilatation as a function of temperature for barium zinc silicates (lines) and relative changes in cell volume as calculated from the values derived from Rietveld calculations (open symbols).

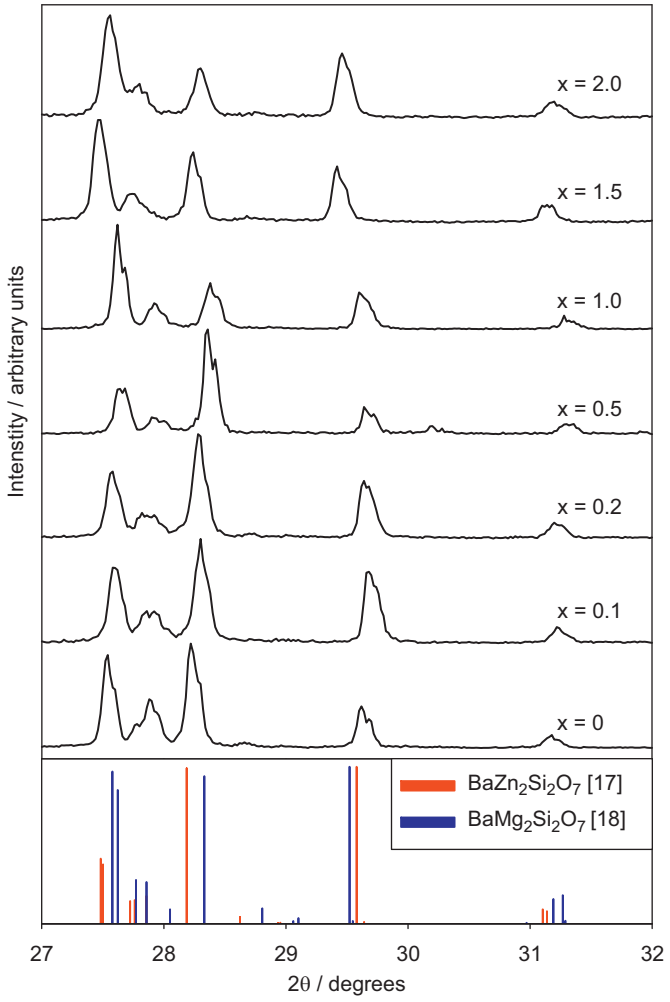

Fig. 6. XRD-patterns of the solid solution series $BaZn_{2-x}Mg_xSi_2O_7$.

Table 3
The values of the technical CTE measured by HT-XRD (α_a, α_b, α_c, α_m) and dilatometer (α_{tech}), in comparison with values from literature (*italics*).

	HT-XRD						Dilatometer	
Sample	α_a (10^{-6}/K)	α_b	α_c	α_m	ΔT (°C)	Ref.	α_{dil} (10^{-6}/K)	ΔT (°C)
$Ba_2ZnSi_2O_7$	8.0	9.1	6.5	8.9	100–800		9.1	100–800
$BaZnSiO_4$	7.0	7.0	15.1	9.7	100–800		10.4	100–800
$BaZn_2Si_2O_7$	25.6	20.7	6.4	17.6	100–300		13.4	100–250
	26.8	*26.1*	*4.3*	*19.1*	*100–300*	[17]	–	
	−21.3	5.3	22.9	2.3	300–800		−3.2	350–800
	−26.3	*7.6*	*25.5*	*2.3*	*300–800*	[17]	–	
	49.1	26.8	−6.2	23.3	100–800		19.1	100–800
	42.9	*28.3*	*−3.4*	*22.6*	*100–800*	[17]	–	

The dilatometric curves for all compounds are shown in Fig. 8 for the solid solution series. All curves show a more or less steep increase of the volume within a comparably small temperature range. As shown above, this increase in volume in the case of the sample which does not contain MgO is due to the transition of a low to a high temperature modification (see above). If MgO was incorporated into the solid solution, this steep increase in volume

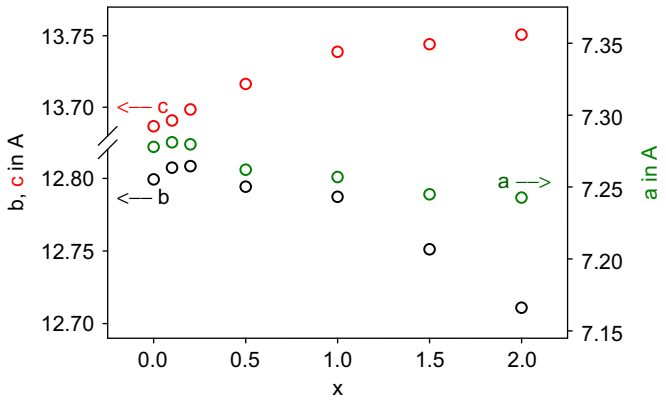

Fig. 7. Cell parameters of the solid solution series $BaZn_{2-x}Mg_xSi_2O_7$.

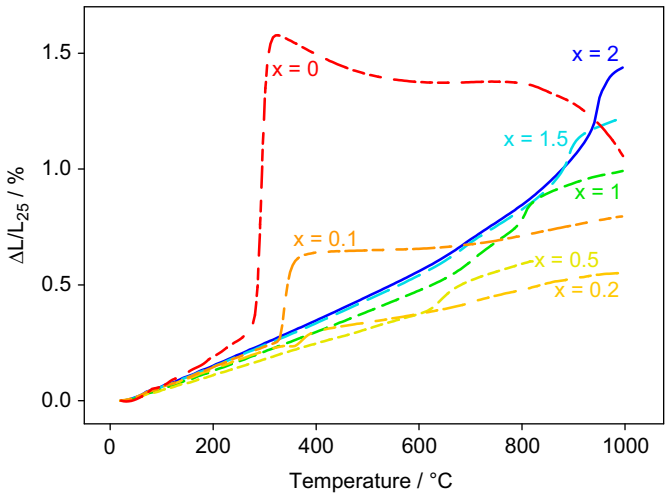

Fig. 8. Dilatation as a function of temperature for the solid solution series $BaZn_{2-x}Mg_xSi_2O_7$.

Table 4
Properties of the samples from the solid solution series $BaZn_{2-x}Mg_xSi_2O_7$.

x in $BaZn_{2-x}Mg_xSi_2O_7$	ρ (g/cm^3)	onset DSC (°C)	onset dil. (°C)	$\alpha_{100-250\ °C}$ (10^{-6}/K)	$\alpha_{100-600\ °C}$ (10^{-6}/K)	$\alpha_{100-800\ °C}$ (10^{-6}/K)
0	4.57	277	276	13.4	26.2[a]	19.1[a]
0.1	4.54	308	334	8.7	12.0[a]	9.3[a]
0.2	4.44	334	379	7.9	6.5[a]	5.9[a]
0.5	4.23	–	623	6.9	6.6	7.8[a]
1.0	4.11	–	797	8.0	8.5	10.3
1.5	3.85	–	873	8.8	9.6	10.9
2.0	3.71	–	937	9.2	10.0	11.2

[a] CTE calculated including the phase transition.

becomes less pronounced and is shifted to higher temperatures (see also Table 4), e.g., from 276 °C for $BaZn_2Si_2O_7$ ($x=0$) to 937 °C for $BaMg_2Si_2O_7$ ($x=2.0$). Up to $x=0.5$, the increase is stronger than for larger x values. Also in the DSC profiles, the phase transition is observed, the attributed onsets of the endothermic signals show a similar trend for the compounds with x in the range from 0 to 0.2, the increase with the x-value, however, is somewhat smaller.

The density of the samples in the solid solution series decreases with increasing Mg-concentration from 4.57 to 3.71 g/cm^3, which is in fairly good agreement with the X-ray density of 4.55 and 3.71 g/cm^3 for $BaZn_2Si_2O_7$ [17] and $BaMg_2Si_2O_7$ [18], respectively.

4. Discussion

Concerning the XRD-measurements, all barium zinc silicates were measured both on a standard sample holder and on a heating stage (see Table 1). The deviations of the room temperature measurements from the values reported in literature (ICSD) were between −0.27 and 0.40%.

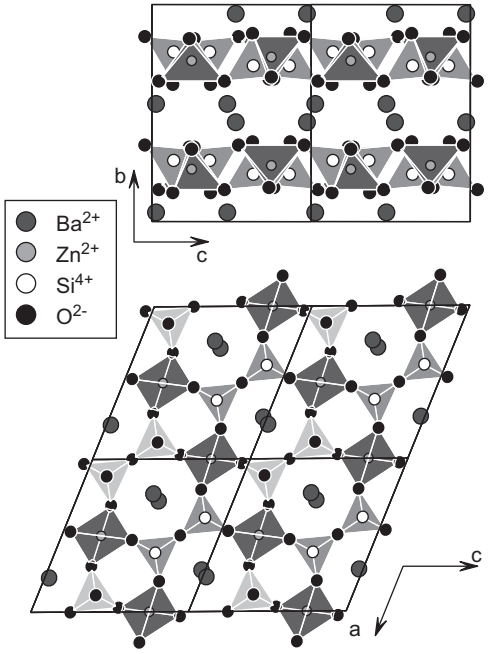

Fig. 9. Crystal structure of $Ba_2ZnSi_2O_7$, as determined by Kaiser and Jeitschko [15]. The upper part of the figure shows a view towards the *bc*-plane, a segment of four unit cells ($2a \times b \times 2c$) is shown. The lower part of the graph shows a view towards the *ac*-plain, only one layer is displayed (that means only 0.5 *b*).

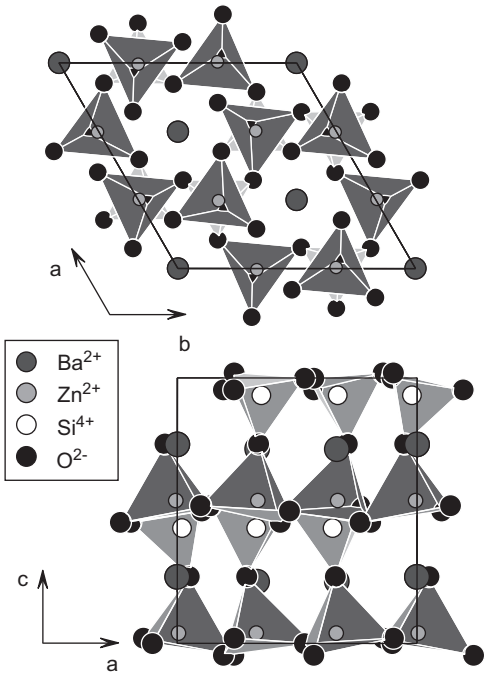

Fig. 10. Crystal structure of $BaZnSiO_4$, as determined by Liu [16]. The upper part of the Figure shows a view towards the *ab*-plain, the lower part shows a view towards the *ac*-plain. One unit cell is shown.

In most cases, the thermal expansion curves derived from HT-XRD and subsequent Rietveld calculations were approximately linear. Only in some cases the temperature dependency was not sufficiently described by a linear fit. Then a quadratic polynomial was preferred. Up to now, from the compositions studied in this paper, in the literature only $BaZn_2Si_2O_7$ has been examined by HT-XRD [17]. Lin et al. reported the cell parameters at various temperatures up to 900 °C. From these data, we calculated the dependencies of the cell parameters on temperature by a polynomial fit (see Table 2 for the fit parameters and Table 3 for the CTEs derived hereof).

For better comparison, the relative changes in the cell parameters were plotted against the temperature (see Fig. 4 and Fig. 5). Although, $Ba_2ZnSi_2O_7$ exhibits only a slight anisotropy of the thermal expansion coefficient, it has a strongly anisotropic structure, as seen in Fig. 9. This compound has a layered structure composed of $[ZnO_4]^{2-}$ tetrahedra connected at each corner to $[SiO_4]$ tetrahedra. Each $[SiO_4]$ tetrahedron is connected over three corners to one $[SiO_4]$ and two $[ZnO_4]^{2-}$ tetrahedra, the forth corner is a non-bridging oxygen atom. The Ba^{2+} ions are located in between the zinc silicate layers in the (0 1 0) plane. The largest thermal expansion is perpendicular to the layers.

As shown in Fig. 10, $BaZnSiO_4$ has a fully cross-linked network of $[SiO_4]$ and $[ZnO_4]^{2-}$ tetrahedra, each tetrahedron connected to four tetrahedra of the other type. The tetrahedra form layers of six-membered rings with all tetrahedra of one type pointing either "up" or "down" along the *c*-axis. Each oxygen in those corners is connected to a next ring lying above or underneath. The rings are stacked over each other to form "channels". The excess negative charge of the $[ZnO_4]^{2-}$ is compensated by the Ba^{2+} ions, which are located in those "channels". This anisotropic structure shows anisotropy in thermal expansion: the largest expansion is parallel to the *c*-axis, i. e., parallel to the channels.

$BaZn_2Si_2O_7$ also possesses an anisotropic structure, as shown in Fig. 11. Chains of $[ZnO_4]^{2-}$ tetrahedra are oriented parallel to the *c*-axis. Furthermore the structure contains di-silicate units $[Si_2O_7]^{6-}$, which are parallel to the *b*-axis. Those chains and di-silicate units are cross-linked to form three-, four- and six-membered rings. The six-membered rings have an oval shape. Each $[ZnO_4]^{2-}$ tetrahedron belongs to two six-membered rings; the plains of two neighboring rings are twisted by 87.4° and 84.4° for the low-temperature and the high-temperature modification, respectively. Each $[SiO_4]$ tetrahedron is connected to three $[ZnO_4]^{2-}$ tetrahedra, hence every di-silicate group belongs to three six-membered rings. The connectivity of the tetrahedral framework does not change during the phase transition, only the orientation of the tetrahedra and the rings formed by them changes. The largest thermal expansion of the low-temperature modification is perpendicular to the $[ZnO_4]^{2-}$ chains and perpendicular to the direction of the di-silicate groups, in the same direction also the largest expansion during the phase transition occurs. A much smaller thermal expansion is observed in the direction of di-silicate groups. By contrast, in the direction of the $[ZnO_4]^{2-}$ chains, a contraction occurs during phase transition, i. e., a negative thermal expansion coefficient is observed. These trends reverse in the expansion of the high-temperature modification: largest expansion is observed parallel to the $[ZnO_4]^{2-}$ chains, negative expansion is observed perpendicular to the $[ZnO_4]^{2-}$ chains and perpendicular to the direction of the di-silicate groups. Thermal expansion coefficients reported in the literature [17] show a fairly good agreement (see Table 3).

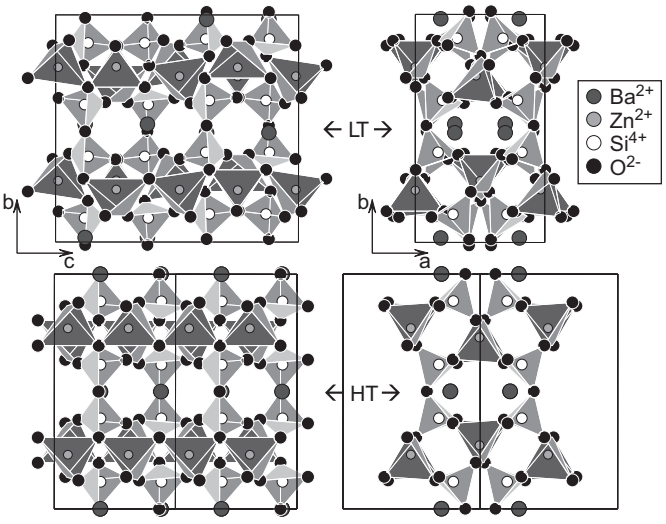

Fig. 11. Crystal structure of $BaZn_2Si_2O_7$, as determined by Lin [17]. The upper part of the Figure shows two views of the low-temperature phase, one unit cell is shown. The lower part shows two views of the high-temperature phase, a segment is chosen that corresponds to the low-temperature phase. The left part of the figure shows a view towards the *bc*-plain, the right part shows a view towards the *ab*-plain.

In the case of polycrystalline samples, CTEs from HT-XRD and dilatometry cannot be compared directly with each other. HT-XRD measures the microscopic expansion of each cell parameter of the unit cell. Dilatometry measures only the sample length of one macroscopic polycrystalline specimen. The temperature dependence of the sample length is not only affected by the thermal expansions in the cell parameters of the unit cell, but also by the orientation of the unit cells (or the grains) to each other and the elastic properties in the respective crystallographic axis. Hence, sample preparation has to be done very carefully to avoid orientation and porosity in the sintered specimens. In the case of $Ba_2ZnSi_2O_7$, $BaZnSiO_4$ and $BaZn_2Si_2O_7$ (up to 320 °C), the sample lengths of the sintered specimens represent very well the mean thermal expansion of the unit cell. In the case of $BaZn_2Si_2O_7$, this correlation is poor above 320 °C. The reason for that behavior is that the samples were not sintered to dense specimens before dilatometry was performed. If this were done, the strong changes in cell dimensions during the phase transition would lead to a rupture of the specimen. Conclusions about the thermal expansion of the high-temperature modification of $BaZn_2Si_2O_7$ hence cannot be drawn from dilatometry.

The introduction of Mg^{2+} into the $BaZn_2Si_2O_7$ lattice leads to a change in various properties. Positions and intensities of the reflections vary, but all powder patterns could be fitted with crystal structure data of $BaZn_2Si_2O_7$, $BaMg_2Si_2O_7$ or $BaZnMgSi_2O_7$ with intermediate values of the cell parameters and the atom position parameters, the positions of M^{2+} (M=Zn, Mg) randomly occupied by Mg^{2+} and Zn^{2+}. The changes in the cell parameters do not show any steep increase or decrease (see Fig. 7) while varying the composition.

The phase transition of $BaZn_2Si_2O_7$ observed by Lin [17] is also found in our own measurements: in HT-XRD, DSC and dilatometry. The phase transition in the solid solution series is proved by both DSC and dilatometry for $x=0$ to 0.2, and by dilatometry for $x=0.5$ to 2.0. The increasing difference between the onset temperatures of DSC and dilatometry (see Table 4) might be caused by the different heating rates and sample geometries.

The solid solution series $BaZn_{2-x}Mg_xSi_2O_7$ with $x>0$ does not show a decrease in dilatation above the phase transition. No rupture in the measured specimens was observed. Hence it is possible to draw conclusions from dilatometry to the thermal expansion of the high-temperature modification. The thermal expansion behavior of the solid solution series is very interesting: while the end members possess a high thermal expansion in the measured temperature range, the samples in between show a

medium ($x=0.1$; 1.0; 1.5) or even fairly low thermal expansion ($x=0.2$; 0.5). If in a crystallizing seal glass $BaZn_2Si_2O_7$ and $BaMg_2Si_2O_7$ are formed, a high thermal expansion can be obtained. When those two phases react with each other due to solid state reactions, some mixed $BaZn_{2-x}Mg_xSi_2O_7$ might form and lead to a degradation of the CTE and to a failure of the seal. Hence, phase formation should be controlled very carefully, also with respect to aging. The thermal expansion coefficients can strongly be affected by minor concentrations of Mg^{2+} if solid solutions are formed.

5. Conclusions

In the temperature range suitable for thermal cycling of solid oxide fuel cells (100–800 °C), $Ba_2ZnSi_2O_7$, $BaZnSiO_4$ and $BaZn_2Si_2O_7$ examined by HT-XRD exhibit CTEs of 8.9, 9.7 and 23.3 · $10^{-6}\,K^{-1}$, respectively. As component of a partially crystalline sealing glass, $BaZn_2Si_2O_7$ is suitable, although the high anisotropy and the large volume expansion caused by the phase transition at 280 °C might be a problem. A partially crystallized seal might additionally contain a glassy phase, or another crystalline phases in the BaO/ZnO/SiO_2-system.

Among the samples of the solid solution series $BaZn_{2-x}Mg_xSi_2O_7$ studied by dilatometry, the CTEs (100–800 °C) are between 5.9 and 19.1 · $10^{-6}\,K^{-1}$. The minimum is reached at $x=0.2$, and also the samples with $x=0.1$ and $x=0.5$ have CTEs too small for application in SOFCs. This might help to understand the mechanisms of failure of such seals containing BaO, ZnO, MgO and SiO_2 during thermal cycling. The samples with $x=1$ to 2.0 match the required CTE range. Especially in the MgO-rich range, the composition can be adjusted to obtain the aimed CTE. Although also the solid solutions exhibit a transition from a low temperature into a high temperature modification, the volume effect which runs parallel is not as pronounced as in the case of the $BaZn_2Si_2O_7$ compound. Hence, it might be interesting to design glass seals near the composition BaO-2 MgO-2 SiO_2.

References

[1] M.K. Mahapatra, K. Lu, Mater. Sci. Eng., R 67 (2010) 65–85.
[2] J.W. Fergus, J. Power Sources 147 (2005) 46–57.
[3] S. Sang, W. Li, J. Pu, L. Jian, J. Power Sources 177 (2008) 77–82.
[4] S. Sang, W. Li, J. Pu, S. Jiang, L. Jian, J. Power Sources 182 (2008) 141–144.
[5] S. Sang, W. Li, J. Pu, C. Bo, L. Jian, J. Power Sources 193 (2009) 723–729.
[6] F. Tietz, Ionics 5 (1999) 129–139.
[7] G.Ch. Kostogloudis, Ch. Ftikos, J. Eur. Ceram. Soc. 19 (1999) 497–505.
[8] F. Tietz, F.J. Dias, B. Dubiel, H.J. Penkalla, Mater. Sci. Eng. B 68 (1999) 35–41.
[9] M. Han, S. Peng, Z. Wang, Z. Yang, X. Chen, J. Power Sources 164 (2007) 278–283.
[10] M. Kerstan, C. Rüssel, J. Power Sources 196 (2011) 7578–7584.
[11] M. Kerstan, M. Müller, C. Rüssel, Mater. Res. Bull. (2011). doi:10.1016/j.materresbull.2011.08.031.
[12] V. Swamy, L.S. Dubrovinsky, F. Tutti, J. Am. Ceram. Soc. 80 (1997) 2237–2247.
[13] E.R. Segnit, A.E. Holland, Aust. J. Chem. 23 (1970) 1077–1085.
[14] M.E. Huntelaar, E.H.P. Cordfunke, J. Nucl. Mater. 201 (1993) 250–253.
[15] J.W. Kaiser, W. Jeitschko, Z. Kristallogr. - New Cryst. Struct. 217 (2002) 25–26. (ICSD 409588).
[16] B. Liu, J. Barbier, J. Solid State Chem 102 (1993) 115–125. (ICSD 73777).
[17] J.H. Lin, G.X. Lu, J. Du, M.Z. Su, C.-.K. Loong, J.W. Richardson Jr, J. Phys. Chem. Solids 60 (1999) 975–983.
[18] C.-.H. Park, Y.-.N. Choi, J. Solid State Chem. 182 (2009) 1884–1888.
[19] D. Taylor, Br. Ceram. Trans. J. 83 (1984) 5–9.